Iron cycling during the autocatalytic decomposition of benzoic acid derivatives by Fenton-like and photo-Fenton techniques

Daniela A. Nichela [a,c,*], Jorge A. Donadelli [a], Bruno F. Caram [a], Ménana Haddou [b], Felipe J. Rodriguez Nieto [a], Esther Oliveros [b], Fernando S. García Einschlag [a,**]

[a] Instituto de Investigaciones Fisicoquímicas Teóricas y Aplicadas (INIFTA, UNLP, CCT La Plata-CONICET), Diagonal. 113 y 64, Sucursal 4, Casilla de correo 16, (B1900ZAA) La Plata, Argentina
[b] Laboratoire des Interactions Moléculaires et Réactivité Chimique et Photochimique (IMRCP), UMR CNRS 5623, Université Toulouse III (Paul Sabatier UPS), 118, route de Narbonne, Toulouse cédex 9 F-31062 France
[c] Instituto da Investigaciones en Biodiversidad y Medio Ambiente (INIBIOMA, CONICET), Centro Regional Universitario Bariloche, Universidad Nacional del Comahue Quintral 1250 (8400) Argentina

ABSTRACT

In the context of our work on the oxidative degradation of a series of hydroxyl derivatives of benzoic acid (HBAs) by Fenton-like and photo-Fenton processes, we present a comprehensive study of the factors that affect the reduction of Fe(III) species, the rate limiting step in the Fenton reaction. We have investigated: (i) the formation of Fe(III)–HBA complexes, (ii) the ability of these complexes to participate in reductive pathways, and (iii) the formation of intermediate products capable of reducing ferric species.

The results show that salicylate-like HBAs form stable bidentate ferric complexes in aqueous solutions at pH 3.0 and that Fe(III) complexation significantly decreases the overall degradation rates in Fenton systems by slowing down Fe(II) production through both dark and photo-initiated pathways. Interestingly, in contrast to ferric complexes of aliphatic carboxylates that undergo a photo-induced decarboxylation upon excitation in the 300–400 nm wavelength range, ferric–salicylate complexes yield Fe(II) and hydroxyl radicals by oxidation of water molecules in the coordination sphere of the metal center. However, their efficiencies are significantly lower than that of the Fe(III) aqua complex. Moreover, Fe(III)–HBA complexes are inert upon excitation of the LMCT bands involving the organic ligand (i.e., 400–600 nm).

As observed for other aromatic compounds, Fe(III)-reducing intermediates formed during the Fenton oxidation of HBAs play a key role in iron cycling. The analysis of the primary oxidation/hydroxylation products as well as Fe(III)-reduction studies showed that, among dihydroxy aromatic derivatives, hydroquinone-like structures were much more efficient than catechol-like structures for reducing Fe(III). Although all trihydroxy derivatives produced Fe(II), ring opening reactions prevailed under the conditions of the Fenton reaction.
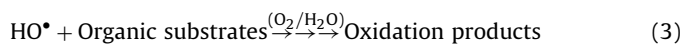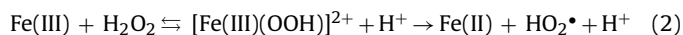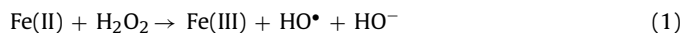
The results of our investigation on the Fenton oxidation of HBA derivatives show that, in each particular case, the complex interplay of the aforementioned factors should be carefully evaluated for developing optimal applications of Fenton processes at a technological level.

© 2015 Elsevier B.V. All rights reserved.

1. Introduction

Interest in advanced oxidation techniques (AOTs) as effective treatments for the oxidation and mineralization of recalcitrant pollutants has been steadily increasing during the last decade. Among AOTs that usually rely on the production of highly oxidizing species such as the hydroxyl radical (HO•), Fenton processes have attracted great interest for technical development due to the relatively low cost of the Fenton reagent (Fe(II)/H_2O_2), the absence of iron toxicity, and the environmentally benign character of H_2O_2 aqueous solutions [1]. The most relevant reactions involved in these systems are [1–3]:

$$Fe(II) + H_2O_2 \rightarrow Fe(III) + HO^\bullet + HO^- \quad (1)$$

$$Fe(III) + H_2O_2 \leftrightarrows [Fe(III)(OOH)]^{2+} + H^+ \rightarrow Fe(II) + HO_2^\bullet + H^+ \quad (2)$$

$$HO^\bullet + \text{Organic substrates} \xrightarrow{(O_2/H_2O)} \text{Oxidation products} \quad (3)$$

* Corresponding author at: Instituto de Investigaciones Fisicoquímicas Teóricas y Aplicadas (INIFTA, UNLP, CCT La Plata-CONICET), Diagonal. 113 y 64, Sucursal 4, Casilla de correo 16, (B1900ZAA) La Plata, Argentina.
** Corresponding author. Tel.: +54 221 425 7291/7430; fax: +54 221 425 4642.
E-mail address: fgarciae@quimica.unlp.edu.ar (F.S. García Einschlag).

The production of HO$^\bullet$ occurs through the decomposition of H_2O_2 in the presence of iron salts (usually inorganic) in acidic medium (Reaction (1)). According to (1), stoichiometric concentrations of HO$^\bullet$ are generated relative to the concentrations of ferrous salts introduced. However, the use of high concentrations of ferrous salts would lead to large sludge amounts of Fe(III) hydroxides [4] undesirable in technological applications. A strategy to minimize the sludge volumes is to use catalytic amounts of Fe(II) or Fe(III) (Fenton-like processes). Nevertheless, since the apparent rate constant of Reaction (2) is much lower than that of Reaction (1), the regeneration of Fe(II) is the rate limiting step in the catalytic iron cycle of most Fenton-like systems, and the overall process efficiencies are strongly dependent on reduction pathways of Fe(III)-species other than the reaction between Fe(III) and H_2O_2 [5].

The reduction of Fe(III) species in Fenton systems may be enhanced through dark and/or photochemical pathways. The reduction rates of Fe(III) species through dark pathways depend on the ambient redox potential of the reaction mixture. C-centered radicals and semiquinone-like intermediates formed as the oxidation proceeds are known to be strong reductants that may participate in the production of Fe(II). Moreover, most aromatic compounds are hydroxylated during their initial oxidation steps, yielding hydroquinone-like intermediates (*ortho-* or *para-* substituted dihydroxybenzenes) that are able to reduce Fe(III) species. Thus, reaction manifolds involving the accumulation of Fe(III)-reducing intermediates usually lead to an autocatalytic behavior since Fe(II) production is substantially increased and the overall process is accelerated [3,5,6]. Another key feature regarding Fenton-like systems is the fact that the efficiency of catalyst recycling is rather sensitive to changes in the coordination sphere of Fe(III) [7] and the presence of Fe(III) chelating agents (e.g. organic pollutants) may substantially affect the production of Fe(II) through dark pathways [7]. For instance, it is well-known that the presence of high oxalate concentrations suppresses the production of hydroxyl radicals in Fenton-like systems operated under dark conditions. In general, as the stability of a given Fe(III)-chelate increases it becomes more difficult to reduce, in some cases in spite of an appropriate standard reduction potential [8,9]. For the latter systems, kinetic restrictions, such as the existence of accessible sites in iron complexes, are also important factors that control the overall reduction rates.

In addition to the contribution of dark pathways, the efficiency of Fe(II) production in Fenton systems highly increases under UV irradiation (see, e.g., [10,11]). The enhancement is mostly due to the photolysis of Fe(III) species, such as aqua complexes and complexes formed with organic ligands, which dissociate in the excited state to yield Fe(II) and the oxidized ligand [1]. The overall rate of the photochemical Fe(II) production depends on the nature and on the spectroscopic properties of the absorbing species as well as on the intensity and the spectral distribution of the incident radiation. For example, although excitation of ligand-to-metal charge transfer (LMCT) bands of Fe(III) aqua complexes leads to the generation of hydroxyl radicals [12,13], the fraction of solar light absorbed by Fe(III) aqua complexes is too small for valuable solar applications to water treatment. Several authors have studied the photochemical behavior of ferric complexes formed with organic ligands [14–16] and shown that natural organic chromophores can greatly enhance Fe(III) reduction rates under solar radiation conditions [17]. This increase in Fe(II) photochemical generation is explained by the shift toward longer wavelengths of the absorption spectra of the complexes formed between Fe(III) and organic ligands with respect to the aqua complexes and by the high quantum yields of Fe(II) photochemical production usually exhibited by ferric complexes of low molecular weight carboxylic acids [14]. As a result, the photolysis of iron complexes with organic ligands, such as carboxylic acids, has been considered for the design of alternative methods for water

treatment. For example, Fe(III)–oxalate [18], Fe(III)–citrate [19], Fe(III)–pyruvate [20] and Fe(III)–ethylenediamine disuccinate [21], have already been used to degrade organic and inorganic pollutants. The photoreactivity of Fe(III) complexes with aliphatic carboxylate and polycarboxylate ligands is well-known and usually leads to decarboxylation of the organic ligand [14,22]. Nevertheless, to the best of our knowledge, studies on the mechanistic behavior of aromatic carboxylic ligands in the photolysis of their ferric complexes have not been reported.

We have previously carried out a comparative study on the oxidation kinetics of hydroxy and hydroxynitro derivatives of benzoic acid (HBAs) in Fenton-like and photo-Fenton systems [6]. 2-hydroxybenzoic (2HBA), 2,4-dihydroxybenzoic (2,4dHBA), 2-hydroxy-5-nitrobenzoic (2H5NBA), 4-hydroxy-3-nitrobenzoic (4H3NBA) and 2-hydroxy-4-nitrobenzoic (2H4NBA) acids were chosen as model substrates for their structural features and because of their high toxicity and relatively low biodegradability. Although the model compounds used were structurally similar, their initial consumption rates were substantially different. Given the aforementioned importance of Fe(III) speciation for the recycling of the catalyst, we here present a detailed study of the formation of ferric complexes with the model substrates and analyze their ability to produce Fe(II) through both dark and photoinduced pathways. The trends are compared with those of well-known Fe(III)–carboxylate complexes formed by aliphatic acids. In addition, since the contribution of Fe(III)-reducing intermediates has a direct bearing on the kinetic profiles of HBAs consumption, we studied both the Fe(III) reduction ability of several polyhydroxy aromatic derivatives and the formation of primary products during Fenton-like treatments of the model HBAs.

2. Experimental

2.1. Reagents

2-Hydroxybenzoic acid (salicylic acid, 2HBA, >98%) and 2,4-dihydroxybenzoic acid (2,4dHBA, ≥98%) were supplied by Fluka, and 2-hydroxy-5-nitrobenzoic acid (2H5NBA, 99%), 4-hydroxy-3-nitrobenzoic acid (4H3NBA, 98%) and 2-hydroxy-4-nitrobenzoic acid (2H4NBA, 97%) were purchased from Aldrich. 2,3,4-trihydroxy-benzoic acid (2,3,4tHBA, 97%, Aldrich), 2,4,5-trihydroxy-benzoic acid (2,4,5tHBA, Discovery$_{cpr}$, Aldrich), 2,4,6-trihydroxy-benzoic acid monohydrate (2,4,6tHBA, >90%, Aldrich), 2,3-dihydroxy-benzoic acid (2,3dHBA, 99%, Aldrich), 2,5-dihydroxy-benzoic acid (2,5dHBA, >98%, Fluka), 2,6-dihydroxy-benzoic acid (2,6dHBA, 98%, Aldrich), 3,4-dihydroxy-benzoic acid (3,4dHBA, Discovery$_{cpr}$, Aldrich) and hydroquinone (HQ, 99%, Fluka) were used for Fe(III)-reduction experiments. All organic reagents were used without further purification. The inorganic reagents H_2O_2 (perhydrol 30%, Merck), H_2SO_4 (98%, Merck), $HClO_4$ (71%, Merck), NaOH (99%, Merck), and Fe(ClO$_4$)$_3$·H$_2$O (chloride <0.01%, Aldrich) were used as received. Solutions were prepared using Milli-Q purified water (Millipore). Great care was taken to prepare Fe(III) stock solutions, which were immediately used, in order to prevent Fe(III) hydroxide precipitation. The pH of the solutions used for complexation, reduction and photolysis experiments was adjusted to 3.0 with $HClO_4$ (0.5 M), whereas for the acid–base equilibrium studies both $HClO_4$ (0.1 M) and NaOH (0.1 M) were used. Mobile phases for LC runs were prepared using HPLC-grade acetonitrile (ACN, Merck), triethylamine (>99%, J.T. Baker), phosphoric acid (H_3PO_4, 85%, Aldrich) and formic acid (HCOOH, 98–100%, Prolabo).

2.2. Analytical methods

Absorption spectra were recorded using a Cary 3 double-beam spectrophotometer from Varian or an HP-8452A diode-array sin-

gle beam spectrophotometer from Hewlett Packard. The pH of the solutions was monitored using a Radiometer pH meter (model PHM220). Quantification of the substrates in the reaction mixtures was performed by HPLC using a Shimadzu instrument (solvent delivery module LC-20AT, online degasser DGU-20A5, UV–vis photodiode array detector SPD-M20A, column oven CTO-10 A5 VP, autosampler SIL-20AAT) equipped with an Alltech Prevail Organic Acid 5 column (RP-C18, 150 mm long × 4.6 mm i.d.). The column temperature was maintained at 25 °C. The mobile phases were prepared by mixing different proportions of ACN with an aqueous buffer at pH 2.0 (58.5 mM H_3PO_4 and 13.0 mM triethylamine). Two mobile phases, composed of 25/75 and 10/90 (v/v) ACN/aqueous buffer were employed, depending on the compound studied. The flow rate was 1 mL min^{-1}. Fe(II) concentrations were quantified by a colorimetric technique through the complex formed with *o*-phenanthroline [23]. LC-MS analyses were performed using a Thermo Finnigan Surveyor MSQ chromatograph, equipped with an interface for electrospray ionization, a quadrupole analyzer and a diode array detector. A Bridge Shield column (RP-C18 125 mm long × 4 mm i.d.) was used. The mass spectrometer was operated in negative ion mode; the spray voltage in the ion source was set to 2.5 kV to the capillary, and the cone voltage was 60 V. Temperature in the spray capillary was 550 °C. Nitrogen was used as nebulizing gas. The mobile phase was a mixture (80/20 v/v) of ACN and a formic acid aqueous solution (0.1%). The system was operated in isocratic mode at a flow rate of 0.5 mL min^{-1}. Prior to injection, all samples were filtered with 0.22 μm nylon filters.

2.3. Chemometric analysis of UV–vis absorption spectra

Spectrophotometric data sets of acid/base and complexation experiments were analyzed by Factor Analysis and Curve Resolution methods. These methods can be applied to bilinear spectroscopic data from a chemical reaction to provide information about composition changes in an evolving system [24,25]. In the present work we chose one of the most widely used algorithms, the alternating least squares method (ALS), which provides estimates of concentrations and spectral profiles simultaneously [25,26]. The ALS algorithm extracts useful information from the experimental data matrix of absorption spectra, $A(r \times w)$, by iterative application of constrained regression analysis using the following matrix product:

$$A = C \times S^T + E \qquad (4)$$

where $C(r \times n)$ is the matrix of the kinetic profiles; $S^T(n \times w)$ is the matrix containing the spectral profiles, and $E(r \times w)$ represents the error matrix. The quantities r, n and w denote the number of recorded spectra, the number of independent species contributing to the total absorbance and the number of recorded wavelengths, respectively. Resolving matrix A may be a rather difficult task since on the one hand, n is usually unknown and on the other hand, curve resolution methods cannot deliver a single solution because of rotational and scale ambiguities [27]. We applied Factor Analysis and Singular Value Decomposition to the experimental matrix for the estimation of n. Initial guesses of individual spectra and concentration profiles were obtained by the Orthogonal Projection Approach [28,29] and Evolving Factor Analysis [28,29]. In order to reduce rotational ambiguities, we used chemically relevant constraints [30] such as mass balance, non-negativity, selectivity and unimodality. Matrix augmentation strategy [26] was used to simultaneously obtain the concentration profiles corresponding to different experimental conditions (i.e., titration spectra obtained with variable metal concentrations ([M]) at fixed ligand concentration ([L]) were jointly analyzed with titration spectra obtained with variable [L] at fixed [M]). Once the normalized spectra and

concentration profiles were obtained, absolute values were calculated using the initial concentrations.

2.4. Experimental procedures and setup

2.4.1. Spectrophotometric characterization of acid–base and complexation equilibria.

The absorption spectra of 2HBA (0.35 mM), 2,4dHBA (0.37 mM), 2H4NBA (0.38 mM), 2H5N (0.38 mM), 3H4NBA (0.36 mM) solutions in the absence of Fe(III) were recorded from pH 1.0 to pH 5.5. Curve resolution methods were used to obtain the distribution functions and the spectral profiles. The pK_a values for carboxylic groups were obtained by nonlinear fitting of the respective distribution functions. The formation of Fe(III)-complexes in aqueous solutions was studied at pH 3.0, using substrate and Fe(III) concentrations ranging from 0 to 3.0 mM and from 0 to 3.5 mM, respectively. The concentration profiles were obtained by analyzing the experimental matrices of UV–vis absorption spectra by the curve resolution methods described in Section 2.3. Conditional formation constants (i.e., at pH 3.0) for the complexes were calculated by nonlinear fitting of the data to the set of equations describing mass balance and complex formation (§ 3.1.2).

#### 2.4.2. Reactivity of Fe(III) species in the presence of hydroquinone as reducing agent

Dark experiments were carried out using HQ as an Fe(III)-reducing agent, at pH 3.0 and 24 ± 1 °C. Aliquots of 0.5 mL of Fe(III) solutions (0.2 mM), freshly prepared in the presence of excess of the different HBAs (2 mM), were reacted with 0.5 mL of HQ solutions (0.1 mM) in 4 mL quartz cells. Control experiments were also performed using aqueous solutions of identical Fe(III) concentration, but in the absence of HBAs. The production of Fe(II) at different reaction times was analyzed by adding 1.5 mL of *o*-phenanthroline as colorimetric reagent and measuring the absorbance values at 510 nm [23].

2.4.3. Photochemical reduction of Fe(III) species

Photochemical experiments were carried out at pH 3.0. In order to avoid the degradation of the ligands by the photoproduced hydroxyl radicals (HO•) [6], the solutions were prepared with an excess of benzene since it is an efficient HO• scavenger and does not form complexes with Fe(III). In addition, ferric solutions in the absence of HBAs were used as control solutions. The initial concentrations of the substrates and Fe(III) varied from 0 to 1.5 mM and from 0.1 to 0.7 mM, respectively. Irradiation experiments were performed in a Pyrex batch reactor equipped with two sampling ports and a recirculation circuit for temperature control (25 ± 3 °C). In this case a medium pressure mercury arc lamp (Philips HPK 125) was used as polychromatic radiation source. All experiments were performed with aerated solutions under continuous stirring and the reagents were kept in the dark before starting irradiation in order to avoid Fe(II) formation during sample preparation and reactor filling.

2.4.4. Analysis of reaction intermediates and reducing ability studies

Fenton-like degradation experiments of each model substrate were carried out in the dark at controlled temperature (24 ± 2 °C). The initial pH of the solutions was adjusted to 3.0. Initial concentrations of the HBAs, Fe(III) and H_2O_2 varied from 0.25 to 2.3 mM, from 0.1 to 1.0 mM, and from 2.0 to 8.0 mM, respectively. All experiments were carried out in a well-stirred batch reactor of 200 mL and under continuous analytic air bubbling. Reaction mixtures were sampled at different reaction times and quenched with MeOH (in order to prevent the degradation of reaction products by hydroxyl radicals produced after sampling). Samples were analyzed by HPLC-DAD
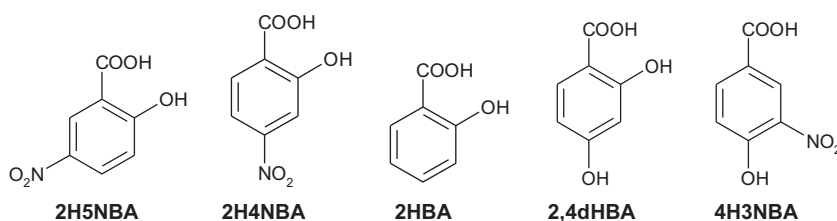
Scheme 1. Chemical structures of the studied benzoic acid derivatives.

and LC-MS. In order to evaluate the Fe(III)-reducing ability of poly-hydroxylated compounds, an additional set of experiments was performed using the same batch reactor at pH 3.0, 24 °C, and under continuous stirring. Ferric solutions were reacted with solutions of different polyhydroxylated compounds structurally related to the intermediate products expected during Fenton-like oxidation of the model HBAs. The initial concentrations of Fe(III)$_{aq}$ and of the polyhydroxylated intermediates varied from 0.2 to 0.8 mM, and from 0.2 to 2.0 mM, respectively. Fe(II) production was evaluated using *o*-phenantroline as colorimetric reagent, whereas the fate of the polyhydroxylated intermediates in the presence of Fe(III)$_{aq}$ was evaluated by HPLC-DAD.

3. Results and discussion

3.1. Formation of Fe(III)-complexes of HBAs in acidic aqueous solutions

3.1.1. Acid base and spectral properties of HBAs in Fe(III) free solutions.

Given that substrate speciation may influence iron cycling in both dark and photo-Fenton systems, the acid–base and spectral properties of the five HBAs were evaluated. The chemical formulas of the studied compounds are presented in Scheme 1.

The absorption spectra of the investigated compounds were recorded for pH values ranging from 1.0 to 5.5 (Fig. S1, Electronic Supplementary information (ESI)). UV–vis spectra were also recorded for inorganic Fe(III) aqua complexes (denoted hereafter as Fe(III)$_{aq}$) at pH values between 1.3 and 4.5 for comparison (data not shown). The acid/base behavior of the latter solutions was in agreement with previously reported results [12]. The pKa of the carboxylic groups (p$K_{a,-COOH}$) and the spectra of the protonated and mono-deprotonated forms of the five HBAs were obtained by the methods described in Sections 2.3 and 2.4. The p$K_{a,-COOH}$ values (Table 1) are in agreement with previously reported data [31–34]. Since irradiation wavelengths above 290–300 nm are of major interest for photo-Fenton systems operated at pH 2.8–3.2, Table 1 also includes information about the absorption bands associated with the lowest energy electronic transitions for the fully-protonated (LH$_2$) and the mono-deprotonated (LH$^-$) forms of the studied HBAs.

The dissociation constant of the carboxyl group is affected by the nature and the position of the substituents. For the salicylic acid derivatives investigated, the presence of the electron withdrawing nitro group significantly lowers the p$K_{a,-COOH}$ with respect to the non-nitrated salicylic acid derivatives.

Although a quantitative analysis of correlations between chemical structure and spectroscopic properties is beyond the scope of the present work, inspection of Table 1 values shows that absorption bands associated with the $S_0 \rightarrow S_1$ electronic transitions of benzoic acid nitro derivatives are centered at longer wavelengths than those of non nitrated substrates. This may be explained by taking into account the expansion of the π system caused by the presence of the nitro group.

3.1.2. Formation of Fe(III) complexes.

The formation of complexes between Fe(III) and the different acids was studied by UV–Vis spectrophotometry at pH 3.0 (near optimal conditions for the Fenton process) [1,10]. Experiments were performed either by varying the ligand (*L* = HBA) concentration at fixed iron concentration or by varying iron concentration at fixed ligand concentration (§ 2.4.1). The aspect of the solutions of the ligands in the absence and in the presence of Fe(III), as well as the absorption spectra in the visible region obtained at different [L]/[Fe(III)] ratios, are given in the ESI (Fig. S2).

Results show that 4H3NBA does not form any complex since the absorption spectrum of the solution does not change in the presence of Fe(III) (Fig. S2, ESI). On the other hand, for the salicylic acid derivatives significant spectral changes were observed within a few seconds after Fe(III) addition, showing that −COOH and −OH groups must be in *ortho* position on the aromatic ring for the formation of ferric complexes. The absorption bands observed for these complexes are typical of ligand-to-metal charge transfer (LMCT) transitions since *d–d* ligand field transitions (LF) are spin forbidden for high spin Fe(III) complexes [6,35].

The absorbance of the solutions containing variable 2,4dHBA or 2HBA concentrations at fixed [Fe(III)] reached a maximum value for ligand concentrations corresponding to equimolar conditions (Fig. S2, ESI). No absorbance changes were found at higher concentrations of 2,4dHBA or 2HBA, indicating that only ferric complexes with 1:1 stoichiometry were formed at pH 3.0. On the other hand, the spectra of the solutions containing 2H4NBA or 2H5NBA at equimolar concentrations with respect to Fe(III) are different from
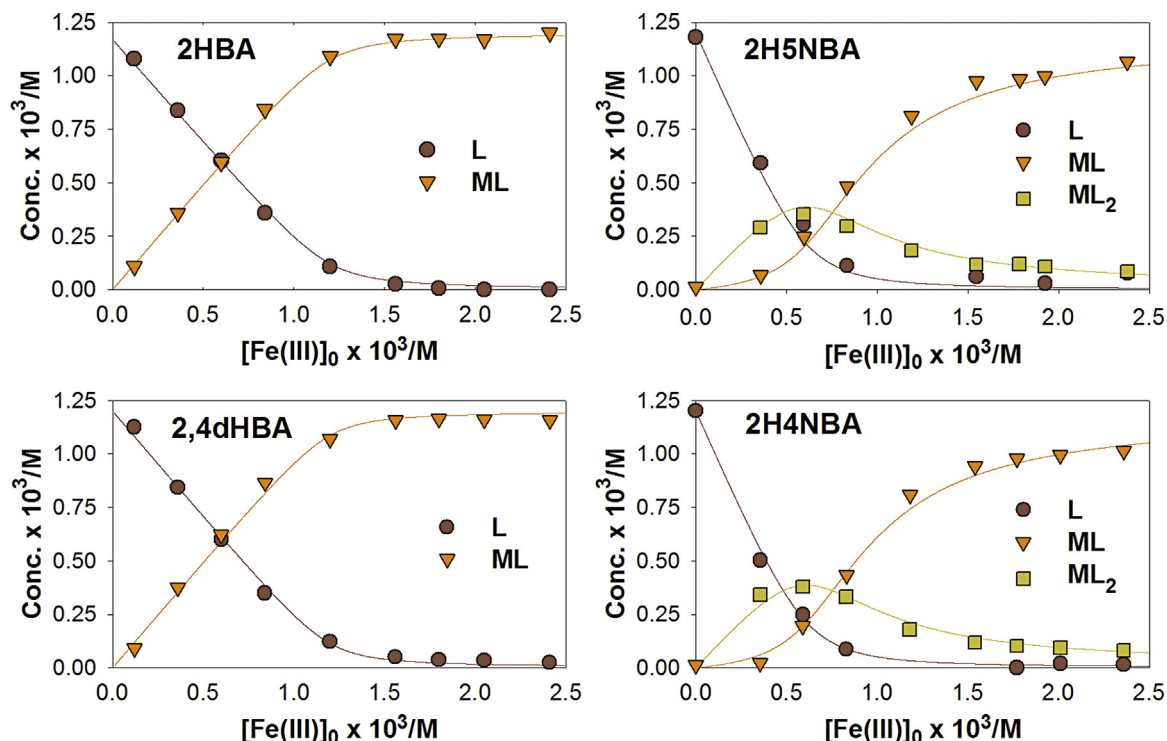
Table 1
Values of p$K_{a,-COOH}$ and spectroscopic data of the lowest energy absorption bands for the studied HBAs (LH$_2$ and LH$^-$: fully-protonated and mono-deprotonated forms, respectively; *L* = HBA).[a]

Compound	p$K_{a,-COOH}$	λ_{max} LH$_2$ (nm)	ϵ_{max} LH$_2$ (M^{-1} cm^{-1})	λ_{max} LH$^-$ (nm)	ϵ_{max} LH$^-$ (M^{-1} cm^{-1})
2H4NBA	1.8 ± 0.1	345	2430	348	2330
2H5NBA	2.1 ± 0.2	310	8240	315	6890
2,4dHBA	2.6 ± 0.2	294	4660	290	4270
2HBA	2.9 ± 0.1	305	3380	295	3280
4H3NBA	3.6 ± 0.1	340	2360	352	2300

[a] Peak wavelengths are given with a precision of ± 2 nm. Relative errors in the absorption coefficients associated with the $S_0 \rightarrow S_1$ transitions are: 2H4NBA: 13.7%; 2H5NBA: 7.2%; 2,4dHBA: 7.0%, 2HBA: 11.9%, 4H3NBA: 9.9%.

Fig. 1. Concentration profiles for the free HBAs (L) and their ferric complexes (ML and ML_2) obtained as a function of $[Fe(III)]_0$ in aqueous solution at pH 3.0 and $[L]_0 = 1.2 \times 10^{-3}$ M.

those obtained in the presence of a large excess of ligand (Fig S2, ESI), thus suggesting the formation of complexes with different stoichiometries.

Previous speciation studies showed that $Fe(OH)^{2+}$ is one of the predominant ferric aqua species at pH 3.0 [36,37], whereas the mono-deprotonated forms are the main ligand species in the HBA–Fe(III) complexes [6]. Therefore, the following reactions of complex formation would be feasible for the 1:1 stoichiometry:

$$LH^- + Fe(OH)^{2+} \leftrightharpoons FeL^+ + H_2O \qquad (5)$$

$$LH^- + Fe(OH)^{2+} \leftrightharpoons Fe(OH)L + H^+ \qquad (6)$$
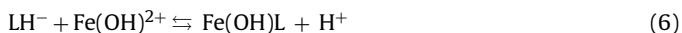
where LH^- and L^{2-} represent the mono-deprotonated and the twice deprotonated forms of the ligand L, respectively. Reaction (6) seems unlikely, since the neutral complex should be rather insoluble and no precipitation was observed during our experiments. Further evidence in favor of Reaction (5) is given in Section 3.2.

In order to estimate the equilibrium constants and to evaluate the stoichiometries of complex formation, the matrices of UV–vis absorption spectra recorded for the different substrates were analyzed using curve resolution methods (Section 2.3). The results confirmed that, within the range of concentrations investigated, 2HBA and 2,4dHBA form only complexes with 1:1 stoichiometry, whereas 2H4NBA and 2H5NBA form complexes with both 1:1 and 1:2 stoichiometries. Fig. 1 shows the concentration profiles for the free ligands (L) and their ferric complexes (ML and ML_2) obtained as a function of $[Fe(III)]_0$.

Conditional stability constants (K′) of the different complexes were estimated by nonlinear regression fitting of the concentration profiles to the following equations:

$$K'_{ML} = \frac{[ML]}{[M] \times [L]} \qquad (7)$$

$$K'_{ML_2} = \frac{[ML_2]}{[ML] \times [L]} \qquad (8)$$

It is important to note that the concentration profiles calculated for the free ligands represent the sum of the concentrations of all protonated and deprotonated forms (i.e., $[L] = [LH_2] + [LH^-] + [L^{2-}]$). Likewise, metal concentration in Eq. (7) corresponds to the total concentration of inorganic ferric species (i.e., $[M] = [Fe^{3+}] + [Fe(OH)^{2+}] + [Fe(OH)_2^+] + 2\,[Fe_2(OH)_2^{4+}]$). Hence, the calculated values are conditional formation constants valid for the experimental conditions used (pH 3.0), since the pH governs both ligand and iron speciation. Table 2 shows the values of K'_{ML} and K'_{ML_2} and information about the absorption bands associated with the LMCT transitions. The distribution coefficients of the mono-deprotonated ligands (αLH^-) were also included for comparison purposes.

Conditional constants indicate relatively strong complexation, the fraction of Fe(III) not complexed by the HBA ligand being lower than 2% under the conditions used in Fenton-like experiments. Values of K'_{ML} follow the order 2HBA < 2,4dHBA < 2H5NBA < 2H4NBA. It is noteworthy that they also increase as the distribution coefficients of the monodeprotonated forms associated with each ligand (αLH^-) increase.

It has been reported that ML_2 and ML_3 complexes can be formed between Fe(III) and 2HBA at pH values higher than 4.0 [38]. The formation of complexes with higher L:M molar ratios is favored at high pH values since increasing pH leads to an increase in the fraction of LH^- forms that participate in Reaction (5). Therefore, the formation of ML_2 species for the nitrated HBAs may be straightforwardly related to their relatively high αLH^- values at pH 3.0 (Table 2).

The analysis of the information about the LMCT bands shows that the complexes formed by the non nitrated ligands exhibit smaller absorption coefficients than those corresponding to the nitrated ones (Table 2). In addition, the former complexes show LMCT bands at longer wavelengths than the latter (violet and red complexes, respectively, Fig. S2, ESI) A similar behavior has been reported for other ferric complexes [38].

Table 2

Log(K') values for complex formation of HBAs with Fe(III), spectroscopic data of the corresponding LMCT bands[a] and distribution coefficient of the mono-deprotonated ligands (αLH^-).

Ligand	log(K'_{ML}) (pH 3.0)	log(K'_{ML2}) (pH 3.0)	λ_{max} ML (nm)	ϵ_{max} ML (M^{-1} cm^{-1})	λ_{max} ML$_2$ (nm)	ϵ_{max} ML$_2$ (M^{-1} cm^{-1})	αLH^- (pH 3.0)
2HBA	4.83 ± 0.04	–	526	1580	–	–	0.56 ± 0.03
2,4dHBA	4.92 ± 0.02	–	520	1390	–	–	0.72 ± 0.04
2H5NBA	4.94 ± 0.08	3.76 ± 0.07	496	2450	486	2800	0.89 ± 0.04
2H4NBA	4.99 ± 0.06	3.93 ± 0.05	486	1790	482	1650	0.94 ± 0.05

[a] Peak wavelengths are given with a precision of ± 2 nm. Relative errors in the absorption coefficients of LMCT bands are: 2HBA: 5.0%; 2,4dHBA: 6.7%, 2H4NB: 4.0%; 2H5NBA: 3.2%.
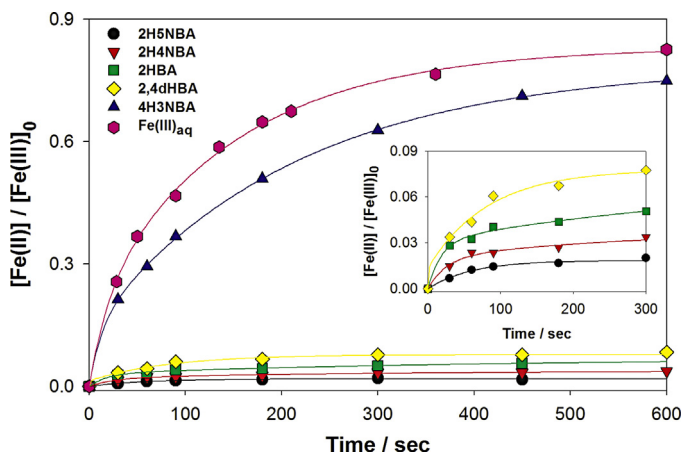

Fig. 2. Hydroquinone-induced Fe(II) production from different ferric species through dark pathways. [Fe(III)]$_0$ = 2.0 × 10^{-4} M, [HQ]$_0$ = 2.0 × 10^{-4} M, [L]$_0$ = 2.0 × 10^{-3} M, pH 3.0 and 24 °C. Fe(III)$_{aq}$ was included for comparison. Inset: Fe(II) production observed in the presence of the ferric complexes during the first 5 min.

3.2. Reactivity of ferric complexes and catalyst recycling

3.2.1. Fe(II) production through non-photochemical pathways

Taking into account that the rate limiting step in most Fenton-like systems is the production of Fe(II) from Fe(III) species, we studied the reduction of the ferric complexes through dark pathways associated with the in situ formation of reducing intermediates. Hydroquinone (HQ) was selected as a model reducing agent, since the hydroxylation of aromatic compounds usually leads to the generation of HQ-like species. Fig. 2 compares the profiles of Fe(II) production obtained for aqueous Fe(III) solutions in the absence and in the presence of the different HBAs.

Interestingly, for all HBAs capable of forming Fe(III) complexes, the fraction of Fe(III) reduced by HQ after 10 min was lower than 12%, whereas Fe(II) production observed for Fe(III)$_{aq}$ was at least 75% within the same timescale. For the tested timescale, the complexes formed with 2H5NBA and 2H4NBA exhibited lower Fe(III) reduction efficiencies (3–5%) than those observed for 2HBA and 2,4dHBA (8–12%). Similar results, reported for Fe(III) complexes of catechol and nitrocatechol [39], were attributed to the lower reduction potential of the complexes formed with the nitrated derivatives. Finally, it should be noted that since 4H3NBA does not form complexes with Fe(III), the Fe(II) production in this case is close to that observed for Fe(III)$_{aq}$ in the absence of HBAs (Fig. 2).

Hence, we have shown that, in line with results reported in the presence of aliphatic chelates such as oxalate [9], Fe(III) reduction may also be suppressed in the presence of strong aromatic complexing agents. These observations have important implications for the kinetics of degradation of organic pollutants in Fenton-like systems. Actually, the ability of ferric species to be reduced appears to be an additional key factor that may drastically affect the autocat-alytic shape of the degradation profiles and the overall reaction rates.

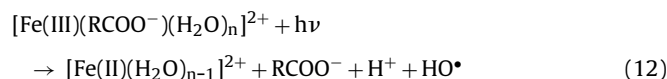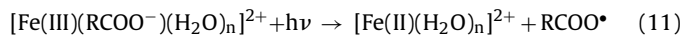#### 3.2.2. Fe(II) production through photochemical pathways

It is well established that Fe(III) usually forms hexa-coordinated, high-spin, labile complexes, which can undergo photochemical reduction of Fe(III) to Fe(II) [6,14]. The overall photo-induced reaction may be written as (charges were omitted for simplicity) [1]:

$$[Fe(III)(L)_n] + h\nu$$
$$\rightarrow [Fe(II)(L)_{n-1}] + L^{\bullet}(L = \text{inorganic or organic ligands}) \quad (9)$$
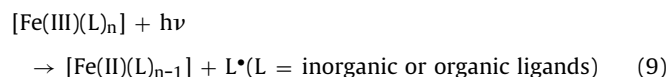
The photochemical redox process involves excitation into the LMCT state as a primary photophysical step. Subsequently, the short-lived LMCT state may yield free Fe(II) and L$^{\bullet}$ outside the solvent cage through the homolytic dissociation of one of the Fe(III)—L bonds [1,40]. The nature of the oxidized species (L$^{\bullet}$) depends on the structure of the ligand. In the predominant Fe(III)–aqua complex at pH 3.0 ([Fe(III)(OH)$^-$]$^{2+}$), the photoreduction of Fe(III) after LMCT excitation ($\lambda \sim 310$ nm) is coupled to the oxidation of HO$^-$ by inner-sphere electron transfer, yielding Fe(II) and HO$^{\bullet}$ (Reaction (10)) [12,40].

$$[Fe(III)(OH)^-]^{2+} + h\nu \rightarrow Fe(II) + HO^{\bullet} \quad (10)$$
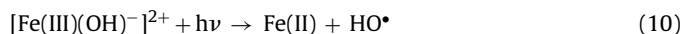
In the case of ferric complexes with organic ligands such as carboxylates and polycarboxylates, the radical generated can be produced from the oxidation of either the organic ligand (Reaction (11)) [18] or a water molecule in the coordination sphere (Reaction (12)). Hence, the photoinduced decomposition of the organic ligand may result either directly by excitation of the complex followed by decarboxylation of RCO$_2^{\bullet}$ (Reactions (11) and (11′)) or indirectly by the electrophilic attack of HO$^{\bullet}$ radicals (Reactions (12) and (3)).

$$[Fe(III)(RCOO^-)(H_2O)_n]^{2+} + h\nu \rightarrow [Fe(II)(H_2O)_n]^{2+} + RCOO^{\bullet} \quad (11)$$

$$RCOO^{\bullet} \rightarrow R^{\bullet} + CO_2 \quad (11')$$

$$[Fe(III)(RCOO^-)(H_2O)_n]^{2+} + h\nu$$
$$\rightarrow [Fe(II)(H_2O)_{n-1}]^{2+} + RCOO^- + H^+ + HO^{\bullet} \quad (12)$$

Aliphatic acids such as oxalate, pyruvate, tartrate and citrate are strong Fe(III)-complexing agents, and it has been established that the photolysis of their ferric complexes takes place through ligand decarboxylation (Reactions (11) and (11′)) [14,41,42]. To the best of our knowledge, comparative studies of HO$^{\bullet}$ photoproduction upon irradiation of ferric complexes with different aromatic ligands have not been reported.

As discussed in the previous section, under our experimental conditions (pH 3.0 and room temperature), the studied HBAs form stable ferric complexes. Stationary irradiation of aqueous solutions of these complexes using wavelengths longer than 450 nm did not

Table 3

Comparison of Fe(II) and phenol (PhOH) initial production rates upon irradiation of ferric complexes of the benzoic acid derivatives and of the Fe(III)-aqua complex (Fe(III) aq) in the presence of benzene as $HO^\bullet$ scavenger. $[Fe(III)]_0 = 1.0 \times 10^{-4}$ M, $[L]_0 = 2.0 \times 10^{-4}$ M, $[benzene]_0 = 1.9 \times 10^{-2}$ M pH 3.0, 24 °C, irradiation at $\lambda > 300$ nm.

HBA Ligand	$r_{Fe(II)}$ (M min^{-1})[a]	r_{PhOH} (M min^{-1})[a]	$r_{Fe(II)}/r_{PhOH}$	$<Abs>_{305-325\,nm}$[c]
2H5NBA	4.7 ($\pm$0.9) x 10^{-7}	4.41 ($\pm$0.16)x 10^{-7}	1.0_7	1.56 ($\pm$0.04)
2H4NBA	7.1 ($\pm$0.8) x 10^{-7}	6.40 ($\pm$0.11)x 10^{-7}	1.1_1	0.45 ($\pm$0.06)
2,4dHBA	2.6 ($\pm$0.3) x 10^{-6}	2.07 ($\pm$0.13)x 10^{-6}	1.2_6	0.32 ($\pm$0.08)
2HBA	2.5 ($\pm$0.4) x 10^{-6}	2.10 ($\pm$0.05)x 10^{-6}	1.1_9	0.29 ($\pm$0.07)
absent[b]	17.0 ($\pm$1.3) x 10^{-6}	17.5 ($\pm$0.1)x 10^{-6}	0.9_7	–

[a] $r_{Fe(II)}$ and r_{PhOH} values were calculated from the profiles of Fe(II) and PhOH formation (see Fig. S4 and the note below in ESI).

[b] Aqueous Fe(III) solution free of organic ligands.

[c] Average absorption due to intra-ligand transitions in the 305–325 nm range.

show any change, neither in the UV–vis absorption spectra nor in the chromatographic profiles. Therefore, excitation of the LMCT bands reported in Table 2 (i.e., absorption bands associated with the charge transfer from the organic ligands to the metal center) did not produce any detectable chemical transformation within the timescale studied. In contrast, irradiation at shorter wavelengths (i.e., down to 300 nm) led to the formation of Fe(II) coupled with the decomposition of both the HBAs and their complexes (Fig. S3, ESI). These results suggest that both the production of Fe(II) and the decomposition of the organic ligands would be initiated by LMCT transitions that involve charge transfer to the metal center from coordinated water molecules, thus yielding $HO^\bullet$ radicals (Reaction (12)).

In order to test the latter hypothesis, we performed a series of irradiation experiments (at $\lambda > 300$ nm) in the presence of benzene as $HO^\bullet$ scavenger (§ 2.4.3), thus minimizing the contribution of secondary dark reactions capable of inducing ligand oxidation and/or Fe(III) reduction by non-photochemical pathways [6,43]. The production of Fe(II) was measured by the o-phenanthroline method [23], whereas the production of hydroxyl radicals was quantified from the amount of benzene transformed into phenol (PhOH)). Under these conditions, HBAs oxidation rates were very low (below 2.5% after 35 min of irradiation). Therefore, it can be concluded that both Reaction (11) and photochemical processes involving $S_0 \rightarrow S_1$ intra-ligand (IL) transitions have a negligible contribution to Fe(III) reduction. Moreover, the initial rates of Fe(II) and PhOH production ($r_{Fe(II)}$ and r_{PhOH}) showed the same trend among the different ferric complexes (Table 3) and their values may be considered equal, within experimental error. Consequently, the photoproduction of Fe(II) by Fe(III)–HBA complexes does not involve decarboxylation pathways (11) and (11'), but proceeds mainly through Reaction (12) producing stoichiometric amounts of $HO^\bullet$ radicals. This is in contrast with the fact that Fe(II) photoproduction proceeds through Reaction (11) for ferric–carboxylate complexes of aliphatic acids [44].

Table 3 shows that, among the different ferric complexes, Fe(III)aq is much more photoactive than the Fe(III)–HBA complexes. It should be noted that $Fe(OH)(H_2O)_5^{2+}$ is the dominant ferric species in the organic ligand-free solutions, whereas iron in Fe(III)–HBA complexes is coordinated by bidentate salicylate-type moieties and by water molecules. Hence, the low photoreactivity observed for the Fe(III)–HBA complexes may explained taking into account two facts: (i) the quantum yield of Fe(II) and $HO^\bullet$ production upon LMCT excitation is higher for $Fe(OH)(H_2O)_5^{2+}$ ($\Phi_{280} = 0.31$) [37] than for $Fe(H_2O)_6^{3+}$ ($\Phi_{254} = 0.065$) [37] because the solvent reorganization energy is lower for HO^- anions than for H_2O molecules [40]; (ii) in solutions of the Fe(III)–HBA complexes, inner filter effects (IFE) are exerted by electronic transitions within the organic ligands (IL transitions, Table 1) since the tail of the LMCT absorption band associated with the Fe(III)—water bond extends to 320–330 nm [12] and the cut-off of the lamp well used is at 300 nm.

Significant differences were observed for $r_{Fe(II)}$ and r_{PhOH} among the Fe(III)–HBA complexes investigated: complexes formed with the non nitrated ligands exhibit higher photoactivities than those formed with nitrated ligands, the efficiency of the Fe(III)–2H5NBA complex being the lowest among the tested compounds. Indeed, inspection of Table 3 shows that the trend observed for $r_{Fe(II)}$ and r_{PhOH} is inversely correlated with the average absorbance of the IL transitions in the 305–325 nm wavelength range ($<Abs>_{305-325nm}$). This suggests that the efficiency of photoinduced oxidation of coordinated H_2O molecules might be relatively independent of the structure of the accompanying bidentate organic ligand.

3.2.3. Photoinduced decarboxylation.

The substantial difference in the photochemical behavior among ferric complexes of aliphatic-carboxy anions and those of aromatic salicylate anions deserves an explanation. Several authors have reported that the removal of one electron from the carboxylate ligands bearing extended π systems requires much lower potentials compared to aliphatic carboxylate ligands [45,46]. Hence, upon excitation of ferric–carboxylate complexes, the formation of R—$COO^\bullet$ radicals through Reaction (11) should be easier for the aromatic compounds tested in the present work than for aliphatic carboxylate ligands. However, the apparent decarboxylation quantum yields may be strongly influenced by secondary processes undergone by R—$COO^\bullet$ radicals. Indeed, back electron transfer to regenerate the initial species (Reaction (13)) competes with decomposition to yield CO2 and carbon centered radicals ($R^\bullet$) (Reaction (11')).

$$RCOO^\bullet + Fe(II) \rightarrow RCOO^- + Fe(III) \qquad (13)$$
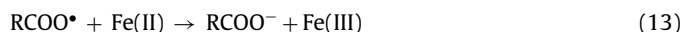
Theoretical calculations show that, although electrons are more easily removed from aromatic carboxylates than from aliphatic ones, decarboxylation of RCOO$^\bullet$ radicals is much more favored for aliphatic carboxyl radicals than for the aromatic ones (see Table S1 and the note below in ESI). Furthermore, it has been reported that the benzoyloxy radical decarboxylates much slower than the acetoxy radical [46,47], the decarboxylation rate constants being $\sim 10^6$ s^{-1} and $\sim 10^9$ s^{-1}, for PhCO$_2^\bullet$ and CH$_3$CO$_2^\bullet$, respectively [47].

3.3. Oxidation mechanism and reaction intermediates

3.3.1. Primary intermediate products

In Fenton systems operated at approx. pH 3.0, the first oxidation step is the $HO^\bullet$ radical addition to the aromatic ring to form hydroxycyclohexadienyl radicals that undergo different reactions to yield the primary oxidation/hydroxylation products (e.g., [1]). Addition of $HO^\bullet$ radicals to aromatic rings bearing deactivating groups (i.e., electron–withdrawing substituents such as —NO$_2$ and —COOH) is mainly statistical in nature [2,48]. However, for aromatic rings bearing activating groups (i.e., electron–donating substituents such as —OH) the electrophilic $HO^\bullet$ addition is mainly directed to ortho and para positions [48]. Moreover, in the presence of both activating

Table 4
Fe(III)$_{aq}$ reducing ability of selected di- and trihydroxybenzoic acid derivatives[a], [Fe(III)]$_0$ = [HBA]$_0$ = 0.8 mM, pH = 3.0 and 24 °C

Compound	CAT-like	HQ-like	RES-like	[Fe(II)]/mM[b]
2,3dHBA	+	–	–	0.74
2,4dHBA	–	–	+	n.d.
2,5dHBA	–	+	–	0.74
2,6dHBA	–	–	+	0.01
3,4dHBA	+	–	–	0.61
2,3,4tHBA	+	–	+	0.76
2,4,5tHBA	+	+	+	0.78
2,4,6tHBA	–	–	+	0.11

[a] CAT-like, HQ-like and RES-like refer to structures bearing two —OH groups in *ortho, para* and *meta* positions, respectively.
[b] The experimental error associated with [Fe(II)] measurements was 0.01 mM.

and deactivating groups, the effect of activating groups prevails [48]. On the other hand, it is important to note that the electrophilic attack of HO• on the carbon bearing the nitro group is rather difficult [2,49], whereas the carboxyl group is much more labile and HO• attack on benzoic acid derivatives may yield decarboxylated products [50–52]. Therefore, for the studied HBAs, the HO• addition is mainly governed by the directing effect of —OH substituents and may occur either on the carbon bearing the carboxyl group (with the corresponding release of CO_2) or on a non substituted position (Scheme S1, ESI).

Fenton-like experiments were performed for the oxidation of the model HBAs under dark conditions. We focused on the analysis of the primary hydroxylation products (§ 2.4.4) since they are mainly responsible for the autocatalytic profiles observed [3,6]. An important difference was observed between the chromatographic profiles associated with the nitrated and the non nitrated HBAs (Fig. S5 a–e, ESI). For the latter, several small and poorly resolved peaks were observed at retention times shorter than 5 min, with the corresponding absorption spectra showing no defined bands beyond 250 nm. In contrast, for the nitrated HBAs, a few important peaks with retention times over 4 min and absorption spectra typical of aromatic compounds were observed. LC-MS profiles showed similar trends. For 2,4dHBA, peaks were detected neither at m/z = 169 (corresponding to the hydroxylation product) nor at m/z = 125 (hydroxylation/decarboxylation product), whereas for 2HBA only important amounts of catechol (hydroxylation/decarboxylation product) and traces of the hydroxylation products at m/z = 153 were found during the entire reaction time. In contrast, for the nitrated substrates, significant signals were observed at m/z = 154 and m/z = 198 corresponding to the expected hydroxylation/decarboxylation and hydroxylation products, respectively. Hence, LC results suggest that the presence of the nitro group somehow stabilizes the aromatic ring toward redox reactions since, under the same conditions, the aromatic intermediates formed from the non nitrated HBAs were readily transformed into ring-opening products.

3.3.2. Reduction of Fe(III) by intermediate products and iron cycling

Three sets of experiments were performed in order to assess the effect of reaction intermediates on iron cycling. In the first set, the Fe(III) reducing ability of several di- and trihydroxybenzoic acids (dHBAs, tHBAs) was tested by reacting aqueous ferric solutions with different dHBAs and tHBAs at pH 3.0 under dark conditions. Table 4 shows the effect of the structural features of the tested compounds on the concentrations of Fe(II) obtained after 2 min of elapsed reaction time. In general, tHBAs showed reducing abilities similar to or higher than structurally related dHBAs. Interestingly, regardless of the position of the hydroxyl groups, all studied tHBAs were capable of reducing Fe(III) to some extent. In contrast, only catechol-like and HQ-like dHBAs were capable
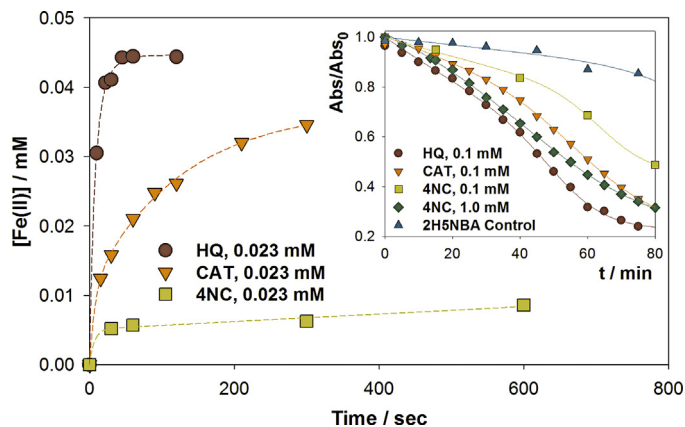

Fig. 3. Dark Fe(II) production obtained in the presence of different dihydroxy aromatic derivatives. [Fe(III)$_{aq}$]$_0$ = 4.4 × 10^{-4} M, [Reducing agent]$_0$ = 0.2 × 10^{-4} M, pH 3.0 and 24 °C. Reducing agents: HQ = hydroquinone, CAT = catechol, 4NC = 4-nitrocatechol. Inset: Normalized absorbance profiles recorded at 315 nm during the autocatalytic degradation of 2H5NBA obtained in the presence of different Fe(III) reducing agents. [2H5NBA]$_0$ = 1 mM, [Fe(III)]$_0$ = 0.1 mM, [H$_2$O$_2$]$_0$ = 5.2 mM.

of producing Fe(II), whereas resorcinol-like compounds showed negligible reactivity toward Fe(III). On the other hand, HPLC-DAD measurements showed no evidence of aromatic compounds after reaction between tHBAs and Fe(III), but suggested the formation of aromatic products after reaction between dHBAs and Fe(III) (data not shown). The latter results indicate that, unlike what was reported for dHBAs [53,54], the oxidation of tHBAs proceeds mainly through ring opening reactions.

Since both HQ-like and catechol-like derivatives are expected to be found among the primary hydroxylation intermediates of HBAs, HQ, catechol (CAT) and 4-nitrocatechol (4NC) were used in a second set of experiments for evaluating the rates of Fe(III) reduction. Fig. 3 compares the kinetic profiles of Fe(II) formation in the presence of equal concentrations of the three additives. Substantially different profiles were observed and the Fe(II) production rates followed the trend: HQ » CAT » 4NC.

Taking into account the latter trend, a third set of experiments was performed to test the effect of the initial addition of HQ, CAT or 4NC on the autocatalytic profiles of 2H5NBA degradation in Fenton-like systems (Inset to Fig. 3). The results showed the same trend as that observed for H$_2$O$_2$ free-solutions, confirming that HQ is more efficient than CAT for the recycling of the catalyst. Moreover, the kinetic profiles suggest that both the nature and the concentration of intermediate reaction products may play a critical role in the degradation efficiency of the HBAs.

3.4. Factors influencing HBAs kinetic profiles in Fenton-like systems

In the previous sections, we presented the results of our studies concerning various key factors that could affect the reduction of Fe(III) species, the rate limiting step in the Fenton oxidation of organic pollutants. The interplay of these factors under the conditions of the Fenton-like and photo–Fenton processes may be very complex. Therefore, we measured the reaction times required for achieving 10% consumption of the different HBA derivatives (t_{10}) in Fenton-like systems (Table 5), and attempted to correlate t_{10} with the four following factors that may play a role in controlling the overall oxidation rates:

(a) *Reactivity toward HO• radicals*

One of the factors not discussed up to now is the efficiency of the reaction of the different HBAs with HO•. The effective rate constants for the latter reaction ($k_{HO•}$) have been calculated from known rate constants [6] as the weighted average of val-

Table 5
Time required for achieving a conversion degree of 10% (t_{10}) in Fenton-like systems for the studied HBAs and related relevant data. ([HBAs]$_0$ = 1 mM, [Fe(III)]$_0$ = 0.1 mM, [H$_2$O$_2$]$_0$ = 5.2 mM).

Compound (C)[a]	t_{10} (min)	$k_{HO^\bullet}$[b] (M^{-1} s^{-1})	Fraction of Fe(III)$_{aq}$ (F_{aq})	Relative Reducibility (RR)	Expected Primary Intermediates[a]	HQL Reductants (Y_{HQL})	CATL Reductants (Y_{CATL})
2H5NBA	58	2.6×10^{10}	0.25%	2.5%	3H-C[c], 4NC[d]	00.0%	100.0%
2HBA	17	2.2×10^{10}	1.61%	6.0%	5H-C[e], 3H-C[e], CAT[e]	33.3%	66.6%
2,4dHBA	7.0	2.2×10^{10}	1.32%	8.5%	5H-C, 3H-C[e], THB[f]	66.6%[g]	33.3%[g]
2H4NBA	6.5	3.1×10^{10}	0.16%	3.5%	5H-C[c], 3H-C[c] 4NC[d]	33.3%	66.6%
4H3NBA	3.3	1.8×10^{10}	100%	90%	5H-C[c], NHQ[d]	50.0%	50.0%

[a] nH–C: hydroxylated derivative of the parent compound with the OH substituent at the position n, 4NC: 4-nitrocatechol, NHQ: nitrohydroquinone, THB: 1,2,4,trihydroxybenzene.

[b] Effective rate constant of the reaction of each compound with hydroxyl radicals under the tested experimental conditions.

[c] A significant peak with the corresponding m/z was detected by HPLC-MS.

[d] Identification by m/z and UV–vis. For CAT and 4NC, retention times of the corresponding standards were also used.

[e] Trace amounts of the corresponding m/z were observed by HPLC-MS.

[f] No significant peaks were observed for the corresponding m/z by HPLC-MS in Fenton systems. However, this compound has been detected during the treatment of 2,4dHBA by VUV photolysis [55].

[g] Note that the HQ-like structures are also CAT-like, but only one of the three structures is purely CAT-like and the effect of HQ-like structures prevails. Moreover, the three structures are trihydroxy benzene derivatives.

ues for complexed and uncomplexed HBAs. The values listed in Table 5 show a rather small range of variation, the largest being for 2H4NBA (3.1×10^{10} M^{-1}s^{-1}) and the smallest for 4H3NBA (1.8×10^{10} M^{-1}s^{-1}).

(b) *Fraction of Fe(III) aq*

Complexation of Fe(III) by organic ligands substantially slows down Fe(II) production (§ 3.2.1). Therefore, the fraction of Fe(III) not complexed by the HBA ligand (F_{aq}) may directly affect the oxidation rates. This fraction is 100% for 4H3NBA, the only HBA investigated remaining as free ligand in Fe(III) aqueous solutions. In contrast, F_{aq} is very small (from 1.61% down to 0.25%) for the other HBAs that form stable bidentate ferric complexes of 1:1 and 1:2 stoichiometries (§ 3.1.2).

(c) *Relative reducibility*

The reactivity of ferric complexes toward reductive pathways may significantly affect the production of Fe(II). The relative reducibility of Fe(III) by HQ (RR) has been used to quantify the effect of the presence of HBA on the Fe(II) production. RR has been calculated as the ratio of the concentrations of Fe(II) measured after 10 min of reaction time, in the presence and in the absence of HBA (data from Fig. 2, § 3.2.1). As expected, the highest RR (90%) was observed in the presence of 4H3NBA, the non-complexing HBA. Among the Fe(III)-complexing substrates, RR is higher in the presence of non nitrated HBAs (6.0–8.5%) than in the presence of nitrated HBAs (2.5–3.5%).

(d) *Reaction intermediates.*

Considering the potential role of the in situ formed intermediates as Fe(III)-reducing agents, the main hydroxylated products detected (§ 3.3.1) have been listed in Table 5 for each HBA. Since resorcinol-like intermediates do not reduce Fe(III) and HQ-like structures (HQL) are more efficient than CAT-like structures (CATL) for the recycling of the catalyst, the expected primary yields of HQL (Y_{HQL}) and CATL (Y_{CATL}) are also indicated in Table 5. The only HBA not yielding any HQL is 2H5NBA.

Inspection of Table 5 shows that t_{10} values vary considerably among the studied HBAs and follow the order: 4H3NBA (3.3) < 2H4NBA (6.5) ≈ 2,4dHBA (7.0) < 2HBA (17) ≪ 2H5NBA (58). The following points stand out from the latter trend:

i) Considering the large differences in t_{10} (from 3.3 to 58 min) and the small range of $_kHO^\bullet$ values (from 1.8 to 3.1×10^{10} M^{-1}s^{-1}), the efficiency of the reaction of the HBAs with hydroxyl radicals does not play any discriminating role in controlling the oxidation rates.

ii) From the values of the two parameters related to Fe(III) complexation (F_{aq} and RR), it would be expected that the non complexing HBA (4H3NBA, F_{aq} = 100% and RR = 90%) would react

considerably faster than all the others, and that the two Fe(III)-complexing nitrated HBAs (2H5NBA and 2H4NBA, F_{aq} < 0.5%, RR < 4%) would be the slowest to undergo oxidation. This is not what is experimentally observed (Table 5). Although the shortest t_{10} among all HBAs was obtained for 4H3NBA and the longest for 2H5NBA, as expected, 2H4NBA reacts similarly to 2,4dHBA and 9 times faster than 2H5NBA. Moreover, while 2,4dHBA and 2HBA display similar F_{aq} and RR values, 2HBA is consumed 2.5 times slower than 2,4dHBA.

iii) Another parameter that strongly influences the kinetic trends is the Fe(III)-reducing ability of the intermediates, which depends on both their structure and their stability (Section 3.3, Fig. 3). Concerning the structure, the primary yield expected for HQ-like intermediates (Y_{HQL}) appears to play a decisive role, whereas the formation of CAT-like intermediates has a minor effect. Indeed, 2,4dHBA and 2HBA should behave similarly according to F_{aq} and RR values (Table 5). However, the higher Y_{HQL} value for 2,4dHBA (66%) than for 2HBA (33.3%) lowers significantly the value of t_{10} for the former (7 min) compared to the latter (17 min), in spite of a higher Y_{CATL} for 2HBA (66%) than for 2,4dHBA (33.3%). Interestingly, 2H5NBA is the only HBA that does not form HQ-like intermediates (Y_{HQL} = 0) and it is oxidized at a considerably lower rate (t_{10} = 58 min) than any other compound (although Y_{CATL} is 100%). Finally, the stability of the Fe(III)-reducing intermediates should also be considered. For instance, Y_{HQL} for 2H4NBA (33%) is lower than for the non nitrated 2,4dHBA (66%), thus it was not expected that both compounds would have similar values of t_{10} (6.5 and 7 min). However, although the trihydroxybenzene derivatives expected to be formed by the first HO$^\bullet$ attack on 2,4dHBA (Scheme S1, ESI) are efficient for Fe(III) reduction (§ 3.3.2), ring opening reactions and decomposition may prevail for this compound (§ 3.3.1).

7. Conclusions

Reduction of Fe(III) is a critical step that controls the activity of the catalyst and the efficiency of degradation of organic pollutants by Fenton and photo-Fenton processes. In this work, we have focused on the elucidation of the main factors preventing or favoring Fe(III) reduction for a series of hydroxy derivatives of benzoic acids (HBAs). The following main conclusions may be drawn from our experimental results:

∗ Complexation of Fe(III) slows down Fe(II) production under dark conditions. This statement is valid not only for aliphatic carboxylates as reported previously in the literature, but also for aromatic

carboxylates as long as they are strong Fe(III)-complexing agents. This is the case of salicylate-like HBAs that form stable bidentate ferric complexes in aqueous solutions at pH 3.0, the optimal pH for the Fenton process.

* In clear contrast to what is usually observed for ferric complexes of aliphatic carboxylates, a rather small photochemical enhancement of the Fenton process should be expected upon irradiation of ferric complexes of aromatic carboxylates. Moreover, this small enhancement is restricted to irradiation in the UV spectral range: under these conditions, excitation of the LMCT bands involving coordinated H_2O molecules and the Fe(III) center leads to the production of stoichiometric amounts of Fe(II) and HO•, but with substantially lower efficiencies than that of the Fe(III) aqua complex. Fe(III)–HBA complexes are inert under visible light irradiation, i.e. upon excitation of the LMCT bands involving the salicylate-like ligand, and no decarboxylation of the latter is observed.

* As observed for other aromatic compounds, Fe(III)-reducing intermediates formed during the Fenton oxidation process of HBAs play a key role in iron cycling and therefore in controlling the overall reaction rates. The efficiency of Fe(III) reduction largely depends on the structure and the amount of the reducing intermediates. In the case of the HBAs investigated, we found that hydroquinone-like structures were much more efficient than catechol-like structures, whereas dihydroxybenzene derivatives with a resorcinol-like structure were unable to reduce Fe(III). In addition, all trihydroxy benzoic acid derivatives efficiently produced Fe(II), but ring opening reactions and decomposition prevailed under the conditions of the Fenton reaction.

The results presented in this work highlight that the autocatalytic profiles and the relative efficiencies of HBAs oxidation in Fenton systems can only be explained by a complex interplay of the following key factors: (i) formation of Fe(III)–HBA complexes, (ii) ability of these complexes to participate in dark and photoinduced reductive pathways, and (iii) formation of intermediate products capable of reducing ferric species. Therefore, in order to develop appropriate kinetic models for the optimal application of Fenton processes at a technological level, these factors should be carefully evaluated for each particular system.

Acknowledgements

Appendix A. Supplementary data

Supplementary data associated with this article can be found, in the online version, at http://dx.doi.org/10.1016/j.apcatb.2015.01.028.

References

[1] J.J. Pignatello, E. Oliveros, A. MacKay, Crit. Rev. Env. Sci. Technol. 36 (2006) 1–84.
[2] L. Carlos, D. Fabbri, A.L.B.P. Capparelli, E. Alessandra, Pramauro, F.S. García Einschlag, Chemosphere 72 (2008) 952–958.
[3] D. Nichela, L. Carlos, F.S. García Einschlag, Appl. Catal. B: Environ. 82 (2008) 11–18.
[4] E. Neyens, J. Baeyens, J. Hazard. Mater. 98 (2003) 33–50.
[5] S. Malato, P. Fernández-Ibáñez, M.I. Maldonado, J. Blanco, W. Gernjak, Catal. Today 147 (2009) 1–59.
[6] D. Nichela, M. Haddou, F. Benoit-Marquié, M.-T. Maurette, E. Oliveros, F.S. García Einschlag, Appl. Catal. B: Environ. 98 (2010) 171–179.
[7] Y. Ohashi, Y. Kan, T. Watanabe, Y. Honda, T. Watanabe, Org. Biomol. Chem. 5 (2007) 840–847.
[8] M. Uchimiya, A.T. Stone, Geochim. Cosmochim. Acta 70 (2006) 1388–1401.
[9] N. Rahmawati, Y. Ohashi, T. Watanabe, Y. Honda, T. Watanabe, Biomacromolecules 6 (2005) 2851–2856.
[10] J.J. Pignatello, Environ. Sci. Technol. 26 (1992) 944–951.
[11] I. Arslan-Alaton, F. Gurses, J. Photochem. Photobiol. A 165 (2004) 165–175.
[12] H.-J. Benkelberg, P. Warneck, J. Phys. Chem. 99 (1995) 5214–5221.
[13] C. Catastini, M. Sarakha, G. Mailhot, M. Bolte, Sci. Total Environ. 298 (2002) 219–228.
[14] L. Wang, C. Zhang, H. Mestankova, F. Wu, N. Deng, G. Pan, M. Bolte, G. Mailhot, Photochem. Photobiol. Sci. 8 (2009) 1059–1065.
[15] M.R.A. Silva, A.G. Trovó, R.F.P. Nogueira, J. Photochem. Photobiol. A 191 (2007) 187–192.
[16] X. Ou, S. Chen, X. Quan, H. Zhao, J. Geochem. Explor. 102 (2009) 49–55.
[17] R.J. Kieber, D.R. Hardison, R.F. Whitehead, J.D. Willey, Environ. Sci. Technol. 37 (2003) 4610–4616.
[18] D. Prato-Garcia, R. Vasquez-Medrano, M. Hernandez-Esparza, Sol. Energy 83 (2009) 306–315.
[19] S.J. Hug, H.-U. Laubascher, Environ. Sci. Technol. 31 (1997) 160–170.
[20] C. Zhang, L. Wang, G. Pan, F. Wu, N. Deng, G. Mailhot, H. Mestankova, M. Bolte, J. Hazard. Mater. 169 (2009) 772–779.
[21] W. Huang, M. Brigante, F. Wu, K. Hanna, G. Mailhot, J. Photochem. Photobiol. A 239 (2012) 17–23.
[22] K. Barbeau, Photochem. Photobiol. 82 (2006) 1505–1516.
[23] M. Rios-Enriquez, N. Shahin, C. Durán-de-Bazúa, J. Lang, E. Oliveros, S.H. Bossmann, A.M. Braun, Sol. Energy 77 (2004) 491–501.
[24] R. Tauler, Chemometr. Intell. Lab. Sys. 30 (1995) 133–146.
[25] M. Garrido, M.S. Larrechi, F.X. Rius, R. Tauler, Chemometr. Intell. Lab. Sys. 76 (2005) 111–120.
[26] M. Garrido, I. Lázaro, M.S. Larrechi, F.X. Rius, Anal. Chim. Acta 515 (2004) 65–73.
[27] A. de Juan, R. Tauler, Anal. Chim. Acta 500 (2003) 195–210.
[28] F. Cuesta Sánchez, S.C. Rutan, M.D. Gil García, D.L. Massart, Chemometr. Intell. Lab. Sys. 36 (1997) 153–164.
[29] R. Tauler, A. de Juan, in: P. Gemperline (Ed.), Practical Guide to Chemometrics, second ed., Taylor & Francis Group, LLC, Greenville, 2006, pp. 417–467.
[30] P.J. Gemperline, E. Cash, Anal. Chem. 75 (2003) 4236–4243.
[31] V.M. Nurchi, T. Pivetta, J.I. Lachowicz, G. Crisponi, J. Inorg. Biochem. 103 (2009) 227–236.
[32] R. Aydin, U. Özer, N. Türkel, Turk. J. Chem. 21 (1997) 428–436.
[33] K.S. Lee, D.W. Lee, Anal. Chem. 46 (1974) 1903–1908.
[34] N. Hirayama, T. Kuwamoto, Anal. Chem. 65 (1993) 141–147.
[35] I.P. Pozdnyakov, V.F. Plyusnin, V.P. Grivin, D.Y. Vorobyev, N.M. Bazhin, S. Pagés, E. Vauthey, J. Photochem. Photobiol. A 182 (2006) 75–81.
[36] H. Gallard, J. De Laat, B. Legube, Water Res. 33 (1999) 2929–2936.
[37] F. Wu, N. Deng, Chemosphere 41 (2000) 1137–1147.
[38] G. Crisponi, V.M. Nurchi, T. Pivetta, J. Inorg. Biochem. 102 (2008) 209–215.
[39] T. Kawabata, V. Schepkin, N. Haramaki, R. Phadket, L. Packer, Biochem. Pharmacol. 51 (1996) 1569–1577.
[40] L. Lopes, J. De Laat, B. Legube, Inorg. Chem. 41 (2002) 2505–2517.
[41] Y. Zuo, J. Hoigné, Environ. Sci. Technol. 26 (1992) 1014–1022.
[42] P. Borer, S.J. Hug, B. Sulzberger, S.M. Kraeme, R. Kretzschmar, J. Phys. Chem. C 111 (2007) 10560–10569.
[43] F. David, G. David, J. Phys. Chem. 80 (1976) 579–583.
[44] C. Weller, S. Horn, H. Herrmann, J. Photochem. Photobiol. A 268 (2013) 24–36.
[45] A. Vogler, A. Kern, Z. Naturforsch. B 34 (1979) 271–274.
[46] L. Eberson, K. Nyberg, J. Am. Chem. Soc. 88 (1966) 1686–1691.
[47] J. Hilborn, J. Pincock, J. Am. Chem. Soc. 113 (1991) 2683–2686.
[48] G. Palmisano, M. Addamo, V. Augugliaro, T. Caronna, A. Di Paola, E. García López, V. Loddo, G. Marcì, L. Palmisano, M. Schiavello, Catal. Today 122 (2007) 118–127.
[49] A. Tauber, H.-P. Schuchmann, C. von Sonntag, Ultrason. Sonochem. 7 (2000) 45–52.
[50] N. Rabaaoui, M.S. Allagui, J. Hazard. Mater. 243 (2012) 187–192.
[51] R.W. Matthews, D.F. Sangster, J. Phys. Chem. 65 (1965) 1938–1946.
[52] G. Albarra, R.H. Schuler, Radiat. Phys. Chem. 67 (2003) 279–285.
[53] J. Xu, R.B. Jordan, Inorg. Chem. 27 (1988) 4563–4566.
[54] R. Liu, B. Goodell, J. Jellison, A. Amirbaham, Environ. Sci. Technol. 39 (2005) 175–180.
[55] K. Azrague, V. Pradines, E. Bonnefille, C. Claparols, M.-T. Maurette, F. Benoit-Marquié, J. Hazard. Mater. 237–238 (2012) 71–78.